

Classical theory of laser-assisted Thomson scattering

Anna K. Puntajer and C. Leubner

Institut für Theoretische Physik, Universität Innsbruck, A-6020 Innsbruck, Austria

(Received 18 January 1989)

Since experimentally feasible configurations of laser-assisted Thomson scattering are quasiclassical, and since semiclassical calculations tend to be lengthy and—in view of the numerous approximations required—lead to results that are difficult to assess, it is demonstrated that the corresponding classical cross section can be derived not only much more simply but also essentially exactly. This cross section, valid for arbitrary intensities of the “assisting” laser field and for arbitrary electron-injection energies, is then graphically compared with semiclassical results from the literature. It shows a published nonrelativistic result to be essentially correct, but its relativistic generalization to be incorrect. As for sum rules, which in the semiclassical literature have only been obtained by recourse to drastic approximations, it is shown that the classical approach straightforwardly yields exact cross sections for the overall laser-assisted Thomson scattering, which again are valid for arbitrary laser intensities and arbitrary electron-injection energies.

I. INTRODUCTION

Laser-assisted Thomson and Compton scattering have been topics of considerable theoretical interest^{1–9} over the years. In this process, a strong laser beam of low-frequency ω_l with a small admixture of vuv or soft-x-ray radiation of frequency ω_x is scattered off a counterpropagating electron beam. Owing to nonlinearities, the scattered radiation contains harmonics $m\omega_l$ ($m = 1, 2, \dots$) of the strong-field frequency as well as combination frequencies $\omega_x + n\omega_l$ ($n = 0, \pm 1, \pm 2, \dots$). It is the cross sections corresponding to these sidebands that one wants to predict.

Apart from one classical analysis by Prakash and Vachaspati,³ all authors have worked within the quantum electrodynamical^{1,4} or the semiclassical framework.^{2,5–9} The corresponding calculations are lengthy and involved, and necessitate numerous approximations, which are difficult to assess and hold potential sources for errors. Moreover, with the exception of Ehlötzky's recent papers,^{8,9} only the cases of the electron being initially at rest in the laboratory frame, and of sideband production in the average electron rest frame have been considered. Although the transformation to the laboratory frame would be straightforward in principle, the drastic approximations involved make it unclear whether first approximating the cross section in the average rest frame and then Lorentz transforming it yields the same result as first Lorentz transforming the cross section and then approximating it in the laboratory frame. This is why Ehlötzky^{8,9} recently performed a semiclassical investigation working in the laboratory frame throughout, and treating separately the cases of nonrelativistic⁸ and relativistic⁹ incident electrons. Yet, again, the results obtained are complicated and expressible only in terms of nontabulated generalized Bessel functions. And, as in all

preceding papers, there is no comparison with related works of other authors.

On the other hand, in the experimentally most interesting case of ω_x being in the vuv or soft-x-ray range, possibly taken from a synchrotron light source, and the assisting field coming typically from an intense Nd-glass laser, a purely classical analysis is adequate.¹⁰ This was recently confirmed by Dobiasch *et al.*¹¹ in the closely related context of the Compton laser, which differs from the present configuration only in that two counterpropagating light beams interact with an electron beam.

The classical approach offers a number of significant advantages. Unlike the semiclassical approach, it is straightforward and requires essentially only a single idealization, namely, the assumption that the incident light beams are plane waves. Hence, it is correct for arbitrary intensities of the strong laser field, and for arbitrary injection energies of the electron beam, which means that a single formula suffices for all cases so far considered in separate semiclassical calculations.

Thus the classical approach constitutes a reliable basis both for predicting experimental observations and for checking published semiclassical results. Indeed, our classical analysis will show some of them to be incorrect, while being experimentally indistinguishable from others. Therefore we briefly review in Sec. II the main steps leading to the exact classical cross section. In Sec. III we present graphical comparisons between the classical results and those of Ehlötzky.^{8,9} For the nonrelativistic case,⁸ we find good agreement for all experimentally accessible intensities of the low-frequency radiation field. In the relativistic case, however, Ehlötzky's cross sections⁹ deviate progressively from the classical ones for increasing laser intensities.

In several investigations, a point of interest has been the derivation of sum rules for the total intensity scat-

tered into a number of harmonics. This topic is taken up in Sec. IV. Whereas semiclassical derivations of sum rules must take recourse to further drastic approximations, which make the interpretation of the resulting expressions difficult, we again find the classical approach to be straightforward and transparent. In particular, no so-called low-frequency approximation is necessary, on which the semiclassical derivation of sum rules seems to hinge.

II. CLASSICAL CROSS SECTION

In calculating the spectral and angular distribution of the photons scattered in a head-on collision of free electrons with an intense two-frequency radiation field, we assume, for convenience, the radiation and electron beams to be exactly counterpropagating, although there would be no difficulty in including a small perpendicular velocity component. We describe the incident radiation fields by plane waves that are linearly polarized along the same direction \mathbf{e}_1 . Hence, the corresponding normalized vector potential may be taken as

$$\begin{aligned}\boldsymbol{\mu}(\eta) &= \frac{eE_1}{m_e c \omega_1} \cos(\omega_1 t - k_1 z) \mathbf{e}_1 \\ &+ \frac{eE_x}{m_e c \omega_x} \cos(\omega_x t - k_x z + \delta) \mathbf{e}_1 \\ &= \left[\mu_l \cos \eta + \mu_x \cos \left(\frac{\omega_x}{\omega_1} \eta + \delta \right) \right] \mathbf{e}_1 = \boldsymbol{\mu}(\eta) \mathbf{e}_1.\end{aligned}\quad (1)$$

In (1), μ_l and μ_x denote the dimensionless intensity parameters of the two waves, and δ a possible phase difference between them. For simplicity, we take ω_x to be an integer multiple of ω_l , $\omega_x = m \omega_l$, since in view of the short pulse duration frequencies are not sharply defined anyway.

Without radiation reaction and with the electron-injection velocity being $-\beta_0 \mathbf{e}_3$, the electron velocity within the laser field is¹²

$$\boldsymbol{\beta}(\eta) = \frac{-2b\boldsymbol{\mu}(\eta) + \mathbf{e}_3[1 - b^2 + \boldsymbol{\mu}(\eta)^2]}{1 + b^2 + \boldsymbol{\mu}(\eta)^2}, \quad (2)$$

with $b = (1 + \beta_0)/(1 - \beta_0^2)^{1/2}$. To calculate the scattering signal, we use the standard formula¹³ for the scattered energy per frequency interval and per unit solid angle,

$$\frac{d^2 I}{d\omega d\Omega} = \frac{e^2}{16\pi^3 c \epsilon_0} \left| \int \frac{\mathbf{s} \times \{[\mathbf{s} - \boldsymbol{\beta}(t)] \times \dot{\boldsymbol{\beta}}(t)\}}{[1 - \mathbf{s} \cdot \boldsymbol{\beta}(t)]^2} \exp\{i\omega[t - \mathbf{s} \cdot \mathbf{x}(t)/c]\} dt \right|^2, \quad (3)$$

where the integral is to be taken over those time intervals during which both pulses interact simultaneously with the electron bunch. Experimentally, one therefore has to synchronize the pulses such that they simultaneously interact with the electron bunch during a common pulse duration τ .

If τ comprises a large number of cycles of the low-frequency beam, it is well known that (3) predicts the scattered radiation to be confined to a sequence of narrow frequency bands,¹² which are due to the interference of the fields scattered during successive cycles of the electron motion. These intensity peaks appear at the frequencies

$$\omega_n = (\omega_x + n\omega_l)/w \geq \omega_l/w, \quad (4)$$

where

$$\frac{d^2 I}{d\omega d\Omega} = \frac{e^2 \tau}{32\pi^4 c \epsilon_0 w} \sum_{n=1-m}^{\infty} \delta(\omega - \omega_n) \left| \frac{\mathbf{s} \times (\mathbf{s} \times \boldsymbol{\beta}_d \mathbf{e}_3)}{1 + s_3 \beta_d} \left[\exp \left[i 2\pi w \frac{\omega}{\omega_l} \right] - 1 \right] + i \frac{\omega}{\omega_l} \mathcal{J} \right|^2, \quad (6)$$

where \mathcal{J} stands for

$$\begin{aligned}\mathcal{J} &= \int_0^{2\pi} \frac{\mathbf{s} \times [\mathbf{s} \times \boldsymbol{\beta}(\eta)]}{1 - \mathbf{e}_3 \cdot \boldsymbol{\beta}(\eta)} \\ &\times \exp \left[i \frac{\omega}{\omega_l} [\eta + (\mathbf{e}_3 - \mathbf{s}) \cdot \mathbf{x}(\eta) \omega_l / c] \right] d\eta,\end{aligned}\quad (7)$$

$$w = \frac{1 - \mathbf{s} \cdot \boldsymbol{\beta}_d}{1 - \mathbf{e}_3 \cdot \boldsymbol{\beta}_d} \quad (5)$$

describes the Doppler shift of the n th sideband. It is produced by the scattering of the incident field off an electron moving with drift velocity $\boldsymbol{\beta}_d$, from the original direction of propagation \mathbf{e}_3 into the direction of observation $\mathbf{s} = (\cos\varphi \sin\theta, \sin\varphi \sin\theta, \cos\theta)$, with $\theta=0$ taken along \mathbf{e}_3 . Since $\boldsymbol{\beta}_d$ is the time-averaged electron velocity (2), which depends on μ_l and μ_x , this Doppler shift is itself intensity dependent. We assume the bandwidth of the detector used to be much larger than the bandwidth of these peaks, so that the detector transmission function may be taken to be constant over the width of one peak. Therefore we are justified to represent the scattered signal as a sequence of δ pulses centered on the frequencies (4) with appropriate amplitudes.¹² This yields

and $\mathbf{x}(\eta)$ is the instantaneous position of the electron resulting from an integration of (2). The two terms within the modulus derive from the usual partial integration of the integral in (3).¹³ The energy scattered per unit solid angle in a particular sideband is then obtained by integrating with respect to frequency over the corresponding δ pulse, to which the integrated part in (6) does not

contribute. In defining the scattering cross section of the n th sideband, $d\sigma_n/d\Omega$, we divide this energy by the incident x-ray intensity per unit area, and by τ . In units of the Thomson cross section σ_{Th} we thus obtain

$$\sigma_{\text{Th}}^{-1} \frac{d\sigma_n}{d\Omega} = \frac{3}{8\pi^3 \mu_x^2 \omega} (\omega_n/\omega_x)^2 |\epsilon_{\perp}(\epsilon_{\perp} \cdot \mathcal{J}_n) + \epsilon_{\parallel}(\epsilon_{\parallel} \cdot \mathcal{J}_n)|^2, \quad (8)$$

where the unit vectors $\epsilon_{\perp} = (\sin\varphi, -\cos\varphi, 0)$ and $\epsilon_{\parallel} = (\cos\varphi \cos\theta, \sin\varphi \cos\theta, -\sin\theta)$ measure the amount of polarization of the scattered radiation perpendicular and parallel to the scattering plane, and \mathcal{J}_n is (7) evaluated at $\omega = \omega_n$. For all realistic sets of parameters, the integral \mathcal{J}_n can be evaluated conveniently and exactly by standard numerical codes. For $\omega_x/\omega_l \gg 1$ and $\mu_x \ll 1$, the cross section (8) turns out to be essentially independent of both the phase difference δ between the strong and weak radiation fields and the intensity parameter μ_x of the x-ray admixture.

III. CLASSICAL VERSUS SEMICLASSICAL RESULTS

Since the most useful comparison between the results of different approaches is a graphical one, and since the most general semiclassical results are due to Ehlitzky,^{8,9} we contrast in this section polar diagrams of the pertinent cross sections. The upper half plane of each figure corresponds to $\varphi = 0$, the lower one to $\varphi = \pi$. Since the cross sections for different sidebands differ by orders of magnitude, different scales are used in different figures. For comparison, the numerical value of the maximum cross section—in whatever direction it occurs—is given in each diagram (in units of the Thomson cross section σ_{Th}), and denoted by σ^{max} .

In comparing Ehlitzky's semiclassical results^{8,9} with the classical one, proper account must be taken of their different definitions, which require the semiclassical quantity to be multiplied by a factor of ω_n/ω_x .¹⁴

Ehlitzky gives both nonrelativistic⁸ and relativistic⁹ versions of the semiclassical cross section in the form of a truncated sum of μ_l -dependent generalized Bessel functions, multiplied by powers of μ_l . For his nonrelativistic cross section,⁸ he also gives a further approximation by retaining only the leading term of this sum. This yields a semiclassical cross section represented by a single generalized Bessel function, which for certain parameter ranges approximately degenerates into an ordinary Bessel function. Where appropriate, all these versions of a particular cross section are collected and contrasted in a single diagram.

Figures 1–3 refer to the sidebands $n = 0, 1$, and 2, respectively. In these figures the classical cross section is labeled (0), Ehlitzky's relativistic semiclassical one⁹ is labeled (1), and his nonrelativistic versions⁸ are labeled (2), (3), and (4), with higher numbers corresponding to a higher degree of approximation. The parameters were chosen as follows: frequency ratio $\omega_x/\omega_l = 100$, Nd-glass laser intensity 1.7×10^{14} W/cm² ($\mu_l = 10^{-2}$), $\mu_x = 10^{-6}$,

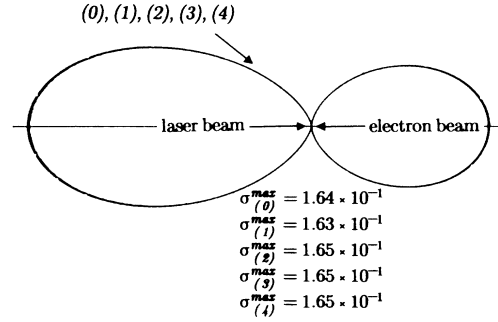


FIG. 1. Classical cross section (0) vs the relativistic semiclassical cross section (1) and the nonrelativistic semiclassical cross sections (2), (3), and (4) (labeled according to increasing degree of approximation) for the central band $n = 0$. The remaining parameters were chosen to be $\omega_x/\omega_l = 100$, $\mu_l = 10^{-2}$, $\mu_x = 10^{-6}$, and $E_0 = 1.6$ keV.

and nonrelativistic electron-injection energy $E_0 = 1.6$ keV ($\beta_0 \simeq 0.08$). For $n = 0$, Fig. 1 shows perfect agreement between the classical and all the semiclassical results. For the first and second sidebands, Figs. 2 and 3, respectively, show nearly perfect agreement between the “exact” classical cross section, (0), and the relativistic and nonrelativistic semiclassical ones, (1) and (2), respectively. In particular, it should be noted that for $\beta_0 \simeq 0.08$ and low intensity $\mu_l = 10^{-2}$, Ehlitzky's relativistic cross section⁹ is consistent with his most accurate nonrelativistic one.⁸ However, the cruder nonrelativistic approximations, (3) and (4), deviate to some extent. Since the findings for the sidebands $n = -1, -2$ are very similar, we omit their graphical representation.

For a frequency ratio $\omega_x/\omega_l = 100$, $\mu_l = 10^{-2}$, $\mu_x = 10^{-6}$, and a relativistic electron-injection energy

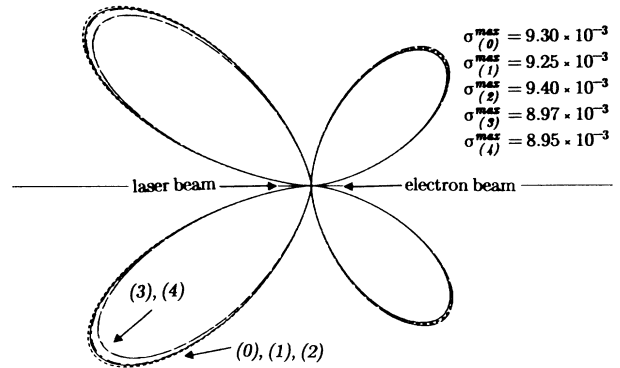


FIG. 2. Classical cross section (0) vs the relativistic semiclassical cross section (1) and the nonrelativistic semiclassical cross sections (2), (3), and (4) (labeled according to increasing degree of approximation) for the sideband $n = 1$. The remaining parameters were chosen to be $\omega_x/\omega_l = 100$, $\mu_l = 10^{-2}$, $\mu_x = 10^{-6}$, and $E_0 = 1.6$ keV.

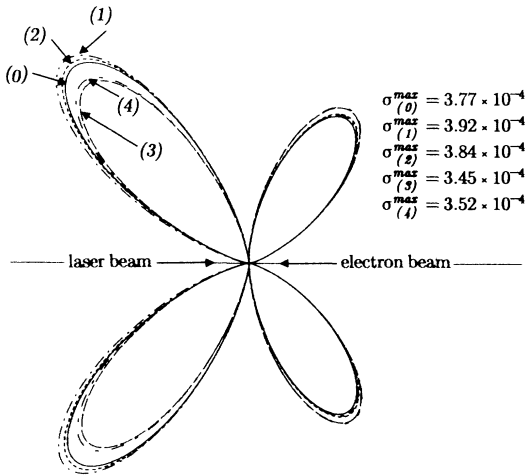


FIG. 3. Classical cross section (0) vs the relativistic semiclassical cross section (1) and the nonrelativistic semiclassical cross sections (2), (3), and (4) (labeled according to increasing degree of approximation) for the sideband $n=2$. The remaining parameters were chosen to be $\omega_x/\omega_l=100$, $\mu_l=10^{-2}$, $\mu_x=10^{-6}$, and $E_0=1.6$ keV.

$E_0=0.5$ MeV ($\beta_0 \simeq 0.86$), Figs. 4–6 exhibit good agreement between the classical cross section, (0), and Ehlotzky's relativistic one, (1), for the sidebands corresponding to $n=0, 1$, and 2 , respectively.

However, for increasing values of μ_l , and for increasing sideband index n , there is a progressive deviation of Ehlotzky's relativistic cross section, (1), from the classical one, (0), both for relativistic and for nonrelativistic electrons (for which it should be equally valid). On the other hand, for nonrelativistic electrons and increasing values of μ_l , his most accurate nonrelativistic cross section, (2), continues to agree. This implies that Ehlotzky's semiclassical cross sections^{8,9} are inconsistent in a range of parameters where they ought to coincide. This can be seen from Figs. 7–9 for the sidebands $n=0, 1$, and 2 , respectively, for a frequency ratio of $\omega_x/\omega_l=100$, a Nd-glass laser intensity of 1.7×10^{16} W/cm² ($\mu_l=10^{-1}$), for $\mu_x=10^{-4}$, and for electrons injected with $E_0=1.6$ keV ($\beta_0 \simeq 0.08$).

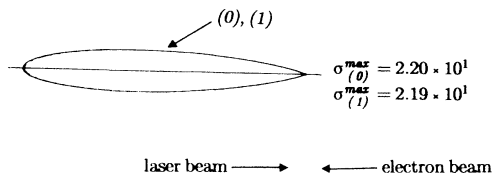


FIG. 4. Classical cross section (0) vs the relativistic semiclassical cross section (1) for the central band $n=0$. The remaining parameters were chosen to be $\omega_x/\omega_l=100$, $\mu_l=10^{-2}$, $\mu_x=10^{-6}$, and $E_0=0.5$ MeV.

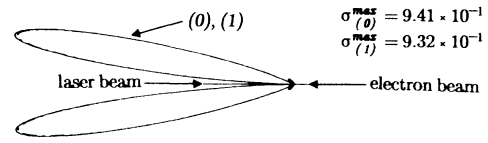


FIG. 5. Classical cross section (0) vs the relativistic semiclassical cross section (1) for the sideband $n=1$. The remaining parameters were chosen to be $\omega_x/\omega_l=100$, $\mu_l=10^{-2}$, $\mu_x=10^{-6}$, and $E_0=0.5$ MeV.

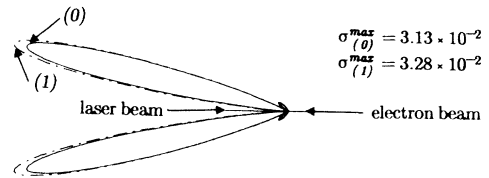


FIG. 6. Classical cross section (0) vs the relativistic semiclassical cross section (1) for the sideband $n=2$. The remaining parameters were chosen to be $\omega_x/\omega_l=100$, $\mu_l=10^{-2}$, $\mu_x=10^{-6}$, and $E_0=0.5$ MeV.

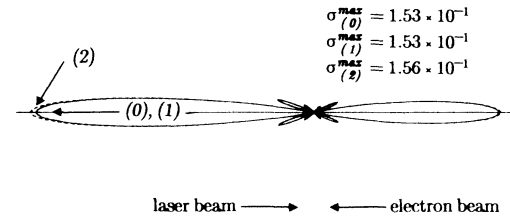


FIG. 7. Classical cross section (0) vs the relativistic semiclassical cross section (1) and the most accurate nonrelativistic semiclassical one (2) for the central band $n=0$. The remaining parameters were chosen to be $\omega_x/\omega_l=100$, $\mu_l=10^{-1}$, $\mu_x=10^{-4}$, and $E_0=1.6$ keV.

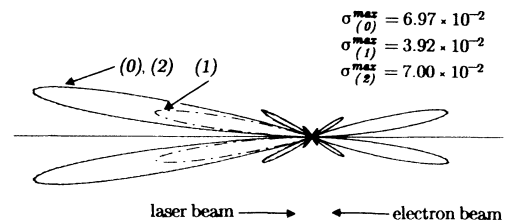


FIG. 8. Classical cross section (0) vs the relativistic semiclassical cross section (1) and the most accurate nonrelativistic semiclassical one (2) for the sideband $n=1$. The remaining parameters were chosen to be $\omega_x/\omega_l=100$, $\mu_l=10^{-1}$, $\mu_x=10^{-4}$, and $E_0=1.6$ keV.

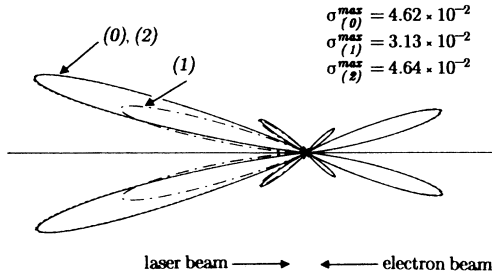


FIG. 9. Classical cross section (0) vs the relativistic semiclassical cross section (1) and the most accurate nonrelativistic semiclassical one (2) for the sideband $n=2$. The remaining parameters were chosen to be $\omega_x/\omega_l=100$, $\mu_l=10^{-1}$, $\mu_x=10^{-4}$, and $E_0=1.6$ keV.

IV. SUM RULES

In the semiclassical literature, two approaches to deriving sum rules can be distinguished.^{5,6,9} In the first,^{5,6} which is only applicable to the case of small intensities, the cross sections for the individual sidebands are crudely approximated by assuming $\mu_l \ll 1$, and then added “by hand.” In the second, pursued by Ehlötzky,⁹ one attempts an analytical summation of all sideband cross sections. In order to succeed, however, one has to resort to the so-called low-frequency approximation, which consists in setting $\omega_l=0$ in some places but not everywhere.⁹ Since the effect of such a hybrid procedure is hard to assess, the result of this summation is difficult to interpret. After all, since contributions from *all* n have been summed, this sum rule includes scattering into harmonics of the laser frequency ω_l . But we will show presently that scattering into harmonics of ω_l greatly dominates that into sidebands of ω_x , so that Ehlötzky’s sum rule⁹ (for which no graphical representation is given) might yield very little information, if any, about the total *laser-assisted* part of Thomson scattering.

In contrast, the classical approach to sum rules is again straightforward and transparent, for neither a low-frequency approximation nor a low-intensity approximation is required. We only need to recall that by Fourier’s theorem, the energy scattered into all harmonics is just

$$\begin{aligned} \frac{dI}{d\Omega} &= \int_0^\infty \frac{d^2I}{d\omega d\Omega} d\omega \\ &= \frac{e^2}{16\pi^2 c \epsilon_0} \int_0^\tau \frac{|\mathbf{s} \times \{[\mathbf{s} - \boldsymbol{\beta}(t)] \times \dot{\boldsymbol{\beta}}(t)\}|^2}{[1 - \mathbf{s} \cdot \boldsymbol{\beta}(t)]^5} dt, \quad (9) \end{aligned}$$

which can also be derived by integrating (3) over all frequencies. Introducing the phase η and dividing by the incident x-ray intensity per unit area, by the pulse duration τ , and by σ_{Th} , we get the total cross section per unit solid angle,

$$\begin{aligned} \sigma_{\text{Th}}^{-1} \frac{d\sigma_{\text{tot}}}{d\Omega} &= \frac{3}{8\pi^2 \mu_x^2} \left[\frac{\omega_l}{\omega_x} \right]^2 \\ &\times \int_0^{2\pi} \frac{|\mathbf{s} \times \{[\mathbf{s} - \boldsymbol{\beta}(\eta)] \times d\boldsymbol{\beta}(\eta)/d\eta\}|^2}{[1 - \mathbf{s} \cdot \boldsymbol{\beta}(\eta)]^5} \\ &\times [1 - \mathbf{e}_3 \cdot \boldsymbol{\beta}(\eta)] d\eta, \quad (10) \end{aligned}$$

where $\boldsymbol{\beta}(\eta)$ is given in (2), and $d\boldsymbol{\beta}(\eta)/d\eta$ is found to be

$$\begin{aligned} \frac{d\boldsymbol{\beta}(\eta)}{d\eta} &= \frac{-2b}{[1 + b^2 + \mu^2(\eta)]^2} \\ &\times \left[\mu_l \sin\eta + \mu_x \left[\frac{\omega_x}{\omega_l} \right] \sin \left[\frac{\omega_x}{\omega_l} \eta + \delta \right] \right] \\ &\times \{ [-1 - b^2 + \mu^2(\eta)] \mathbf{e}_1 + 2b\mu(\eta) \mathbf{e}_3 \}. \quad (11) \end{aligned}$$

Since the numerical evaluation of the integral (10) is straightforward, we make no attempt to expand it in powers of μ_l . [Note that because (10) is independent of the phase difference δ , only even powers of μ_l would enter such an expansion. The point is that the particular value $\delta=\pi$ corresponds to a sign reversal of μ_l , and independence of this sign reversal implies a dependence on the modulus of μ_l only.]

Equation (10) is, of course, not yet a sum rule for laser-assisted Thomson scattering, since it includes strong contributions from scattering into harmonics of ω_l . In order to isolate the total cross section stemming from laser-assisted Thomson scattering alone, we subtract from Eq. (10) the analogous expression corresponding to the case of only the strong laser being present,

$$\frac{d\sigma_{\text{LA}}(\mu_l, \mu_x)}{d\Omega} = \frac{d\sigma_{\text{tot}}(\mu_l, \mu_x)}{d\Omega} - \frac{d\sigma_{\text{tot}}(\mu_l, 0)}{d\Omega}, \quad (12)$$

normalizing, of course, the two cross sections on the right-hand side in the same way, namely, as chosen in Eq. (10). This leads to a meaningful result, because one finds by inspection that to a high accuracy the scattering into harmonics of ω_l is insensitive to the presence of a small high-frequency admixture.

Figures 10–12 are again polar representations with the

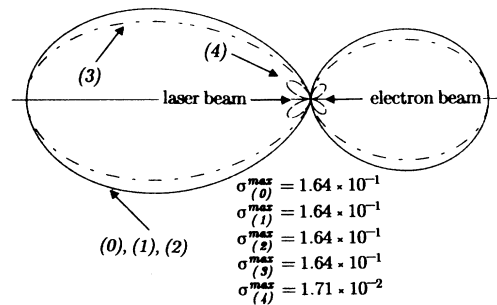


FIG. 10. Overlapping graphs of overall laser-assisted Thomson cross sections, (0) and (1), and linear Thomson cross section, (2). For a small assisting intensity of $\mu_l=10^{-2}$, these graphs are the sum of the cross sections for scattering into the central band $n=0$, (3), and into either of the sidebands $n=\pm 1$, (4). The remaining parameters were chosen to be $\omega_x/\omega_l=100$, $\mu_x=10^{-6}$, and $E_0=1.6$ keV.

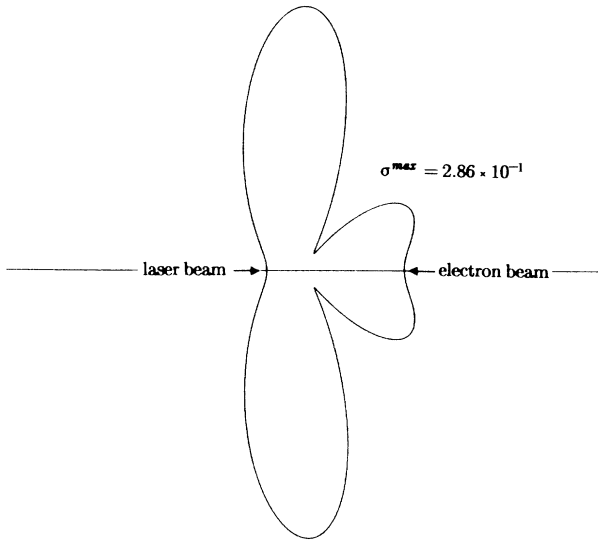


FIG. 11. Overall laser-assisted Thomson cross section, Eq. (12), for a very high assisting intensity of $\mu_l = 1$. The remaining parameters were chosen to be $\omega_x/\omega_l = 100$, $\mu_x = 10^{-4}$, and $E_0 = 1.6$ keV.

upper half plane corresponding to $\varphi = 0$, and the lower one to $\varphi = \pi$. Throughout these figures, we assume a frequency ratio of $\omega_x/\omega_l = 100$, and a nonrelativistic electron-injection energy of 1.6 keV ($\beta_0 \approx 0.08$). Information about the scale used in each figure is given as before by σ^{\max} , denoting the maximum value of whatever cross section is depicted.

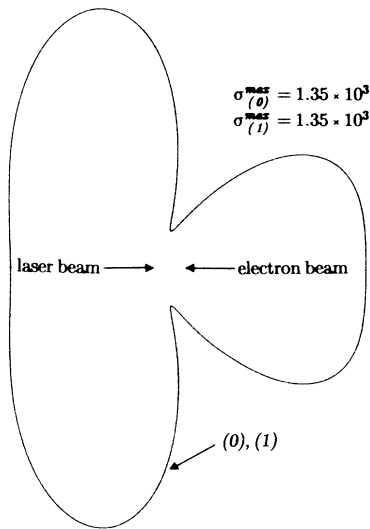


FIG. 12. Overlapping graphs of the “sum rule,” Eq. (10), with (0) and without (1) a small high-frequency admixture of $\mu_x = 10^{-4}$. The remaining parameters were chosen to be $\omega_x/\omega_l = 100$, $\mu_l = 1$, and $E_0 = 1.6$ keV.

Figure 10 refers to a Nd-glass laser intensity of 1.7×10^{14} W/cm² ($\mu_l = 10^{-2}$), and to a high-frequency admixture of $\mu_x = 10^{-6}$. The solid curve shown actually consists of three overlapping curves. Firstly, it represents the sum rule for laser-assisted Thomson scattering [labeled (0)] as derived by subtraction from Eq. (12). Secondly, it represents the result of a summation of the sidebands $n = -3$ to $n = 3$ “by hand” [labeled (1)]. This establishes our above claim that Eq. (12) indeed yields the correct sum rule for laser-assisted Thomson scattering. Thirdly, it represents the cross section for Thomson scattering with respect to ω_x in the absence of the strong radiation field [labeled (2)]. On the other hand, the two dashed lines correspond to laser-assisted Thomson scattering into the central band $n = 0$ [labeled (3)], and into either of the sidebands $n = \pm 1$ [labeled (4)], respectively. Hence, for relatively small values of μ_l , sideband production in laser-assisted Thomson scattering takes place at the “expense” of the central band $n = 0$, a fact that has already been briefly mentioned in Refs. 5 and 6. From the experimental point of view, the overall laser-assisted Thomson scattering is an unsuitable measure of the nonlinearity of the process, since for practical values of μ_l it is indistinguishable from linear Thomson scattering in the absence of a strong laser field. In the case of an imperfect overlap of the strong and weak radiation fields, we would therefore observe pretty much the same signal, independent of the strong laser being on or off. Scattering into the sidebands themselves, however, only occurs when both fields are on.

It is of interest to investigate whether this near equality of linear Thomson scattering and overall laser-assisted Thomson scattering persists for increasing intensities of the strong laser field. We therefore consider next a deliberately unrealistic intensity parameter of $\mu_l = 1$. For such intensities, the method of Eq. (12) is far more convenient for obtaining the overall laser-assisted Thomson cross section than summing “by hand” over the sidebands, since now a large number of these contribute significantly. Assuming $\mu_x = 10^{-4}$, the result is shown in Fig. 11. It should be noted that the left-hand side of Eq. (12) is roughly a factor of 5×10^3 smaller than the individual terms on the right-hand side, which are of the order of 10^3 . This underlines the fact that the “sum rule” Eq. (10) is vastly dominated by scattering into harmonics of the laser frequency ω_l . These individual terms are shown in Fig. 12 as an overlapping double curve, where the results of the evaluation of Eq. (10) with and without a small high-frequency admixture are labeled (0) and (1), respectively. Again we verified that the production of harmonics in the neighborhood of ω_l is almost independent of the value of μ_x (for $\mu_x = 10^{-4}$ and $\mu_x = 0$, the maximum absolute difference in the production of the first harmonic was found to be roughly 4×10^{-6}), so that the difference of the two terms on the right-hand side of Eq. (12) is entirely due to the laser-assisted sideband production in the neighborhood of ω_x .

By contrasting the angular patterns and the scale lengths σ^{\max} in Figs. 10 and 11, we see that the overall laser-assisted Thomson scattering is strongly dependent

on the intensity parameter μ_l of the "assisting" low-frequency laser field.

V. CONCLUSIONS

The graphical comparisons in Sec. III confirm our initial claim that in situations that are currently experimentally feasible, the classical analysis of laser-assisted

Thomson scattering is perfectly adequate. However, if we compare the ease of the derivation of the classical results with the labor required for the semiclassical ones, the classical approach is greatly superior. This is particularly true for sum rules, where on the semiclassical level one has to go through very lengthy calculations, arriving at last at rather unclear results for small values of μ_l , while no semiclassical sum rule at all has so far been given for $\mu_l \simeq 1$.

¹Z. Fried and W. M. Frank, *Nuovo Cimento* **27**, 218 (1963).

²V. P. Oleinik, *Zh. Eksp. Teor. Fiz.* **53**, 1997 (1967) [*Sov. Phys.—JETP* **26**, 1132 (1968)].

³H. Prakash and Vachaspati, *Nuovo Cimento* **53B**, 24 (1968).

⁴H. Prakash and Vachaspati, *Nuovo Cimento* **53B**, 34 (1968).

⁵R. Guccione-Gush and H. P. Gush, *Can. J. Phys.* **53**, 2326 (1975).

⁶A. I. Akhiezer and N. P. Merenkov, *Zh. Eksp. Teor. Fiz.* **88**, 72 (1985) [*Sov. Phys.—JETP* **61**, 41 (1985)].

⁷F. Ehlotzky, *Opt. Commun.* **25**, 221 (1978).

⁸F. Ehlotzky, *J. Phys. B* **20**, 2619 (1987).

⁹F. Ehlotzky, *J. Phys. B* **22**, 601 (1989).

¹⁰C. S. Shen, *Phys. Rev. D* **17**, 434 (1978).

¹¹P. Dobiasch, M. V. Fedorov, and S. Stenholm, *J. Opt. Soc. Am. B* **4**, 1109 (1987).

¹²C. Leubner and F. Ehlotzky, *J. Phys. A* **11**, 759 (1978).

¹³J. D. Jackson, *Classical Electrodynamics* (Wiley, New York, 1975), Chap. 14.

¹⁴F. Ehlotzky, *Acta Phys. Austriaca* **31**, 31 (1970).